

ARTICLE

<https://doi.org/10.1038/s42004-018-0096-x>

OPEN

Strong defocusing of molecular reaction times results from an interplay of geometry and reaction control

Denis S. Grebenkov ¹, Ralf Metzler ² & Gleb Oshanin ³

Textbook concepts of diffusion-versus kinetic-control are well-defined for reaction-kinetics involving macroscopic concentrations of diffusive reactants that are adequately described by rate-constants—the inverse of the mean-first-passage-time to the reaction-event. In contradiction, an open important question is whether the mean-first-passage-time alone is a sufficient measure for biochemical reactions that involve nanomolar reactant concentrations. Here, using a simple yet generic, exactly solvable model we study the effect of diffusion and chemical reaction-limitations on the full reaction-time distribution. We show that it has a complex structure with four distinct regimes delineated by three characteristic time scales spanning a window of several decades. Consequently, the reaction-times are defocused: no unique time-scale characterises the reaction-process, diffusion- and kinetic-control can no longer be disentangled, and it is imperative to know the full reaction-time distribution. We introduce the concepts of geometry- and reaction-control, and also quantify each regime by calculating the corresponding reaction depth.

¹Laboratoire de Physique de la Matière Condensée (UMR 7643), CNRS— Ecole Polytechnique, University Paris-Saclay, 91128 Palaiseau, France. ²Institute of Physics & Astronomy, University of Potsdam, 14476 Potsdam-Golm, Germany. ³Sorbonne Université, CNRS, Laboratoire de Physique Théorique de la Matière Condensée (UMR CNRS 7600), 4 place Jussieu, F-752525 Paris Cedex 05, France. Correspondence and requests for materials should be addressed to R.M. (email: rmetzler@uni-potsdam.de)

Reactions between chemically active molecules in condensed matter systems are typically controlled by two factors: the diffusive search of the species for each other^{1–4} and the intrinsic reactivity κ associated with the probability that a reaction indeed occurs when the particles collide with each other⁵. For chemical reactions involving sufficiently high concentrations of particles, which are initially uniformly distributed in the container or reactor such that encounters between reactive species occur more or less uniformly in time, theories based on mean effective reaction rates provide an adequate description of the reaction kinetics^{1–3}—apart from some singular and well-known reaction schemes which exhibit anomalous, fluctuation-induced kinetics under special physical conditions (see, for instance refs. 4,6–11). Since the seminal works by Smoluchowski¹² and Collins and Kimball¹³ a vast number of theoretical advances have scrutinised a combined effect of both rate-controlling factors on the mean effective rates providing a comprehensive understanding of this effect^{1–4,14–17}. In particular, the mean reaction time is the sum of two time scales corresponding to the inverse diffusion coefficient and the inverse intrinsic reactivity (see Eq. (5)), such that the influence of diffusion control and (chemical) rate control are separable¹³.

For many biochemical reactions, however, the reactive species do not exist in sufficiently abundant amounts to give rise to smooth concentration levels. In contrast, only small numbers of biomolecules, released at certain prescribed positions, are often involved in the reaction process. Indeed, in systems such as the well-studied Lac and phage lambda repressor proteins only few to few tens of molecules are typically present in a living biological cell, corresponding to nanomolar concentrations. The starting positions of biomolecules can either be rather close to the target or relatively far away. Particularly in the context of the rapid search hypothesis of gene expression, it was shown that the geometric distance between two genes, communicating with each other via signalling proteins, is typically kept short by design in biological cells¹⁸, guaranteeing higher-than-average concentrations of proteins around the target in conjunction with fast and reliable signalling¹⁹. Quite generically, many intracellular processes of signalling, regulation, infection, immune reactions, metabolism or transmitter release in neurons are triggered by the arrival of one or few biomolecules to a small spatially localised region^{20,21}. In such cases, it becomes inappropriate to rely on mean rates, and one needs to know the whole distribution of random reaction times, also called the first passage times to a reaction event. Lacking a large number of molecules, reaction times become strongly defocused such that the mean reaction time is no longer representative and the most probable reaction time becomes relevant. We note that even for perfect reactions that occur immediately upon the first encounter between two particles and have thus infinitely large intrinsic reactivity, the mean and the most probable first passage times can differ by orders of magnitude^{22,23} and two first passage events in the same system may be dramatically disparate^{24–26}.

For such effectively few-body reactions, most of the available theoretical effort has been concentrated on the analysis of perfect reactions and hence, on the impact of diffusion control only^{27–29}. In particular, in ref. 28, it was argued that for perfect reactions the reaction time density (RTD) can be accurately modelled as

$$H(t) \approx q\delta(t) + (1 - q)\exp(-t/t_{\text{mean}})/t_{\text{mean}}, \quad (1)$$

where t_{mean} is the MFPT and q is the contribution of trajectories that arrive to the target site immediately. Conversely, fluctuations of the cycle completion time for enzymatic reactions, in absence of any diffusion stage, have been quantified through the coefficient of variation, γ , of the corresponding distribution function of

these times³⁰. Few other works^{31–35} analysed the combined effect of both rate-controlling factors, but solely for the mean reaction time. These works have shown that the effect of the intrinsic reactivity is certainly significant and even most likely is the dominant factor. The question of the combined influence of both factors on the full distribution of reaction times has been only addressed most recently³⁶, with the focus on the target search kinetics in cylindrical geometries. However, the results of Grebenkov et al.³⁶ rely on the so-called self-consistent approximation³¹ and moreover, have a somewhat cumbersome and thus less practical form. Hence, it is highly desirable to consider particular yet generic examples for which the RTD can be calculated exactly and the results can be presented in a lucid, compact and easy to use form revealing numerous insightful features well beyond the simple approximation in Eq. (1). This is clearly an appealing problem of utmost significance for a conceptual understanding of the kinetics of biochemical reactions.

We here focus on the conceptually and practically relevant question of the influence of the intrinsic chemical reactivity and the initial position of the reacting particles onto the form of the full distribution of reaction times. We demonstrate that when the reactivity is finite and no longer guarantees immediate reaction on mutual encounter, the defocusing of reaction times is strongly enhanced. Remarkably, an extended plateau of the reaction time distribution emerges due to this reaction control, such that the reaction times turn out to be equally probable over several orders of magnitude. A direct consequence of the defocusing is that the contributions of diffusion and rate effects are no longer separable. To distinguish them from the classical concepts of diffusion and kinetic control, we will talk about geometry (initial distance) control and reaction (intrinsic reaction rate) control, keeping in mind that the latter not only specifies the dominant rate-controlling factor for the MFPT, but affects the shape of the full RTD. An exact solution for the RTD provides us a unique opportunity to derive explicit formulae, for arbitrary initial conditions and arbitrary values of the intrinsic reaction constant κ for several characteristic properties of the distribution such as, e.g., its precise functional forms in different asymptotic regimes, the corresponding crossover times between these kinetic regimes, and also the reaction depths corresponding to these time scales.

Results

Mathematical model. We consider a model involving a pair of reactive molecules: a partially absorbing, immobile target site of radius ρ within a bounded domain of radius R limited by an impenetrable boundary, and a molecule, initially placed at some prescribed position and diffusing with diffusivity D . Once the diffusing particle hits the surface of the target site, it reacts with (binds to) the latter with a finite, intrinsic reaction rate κ . The reflecting outer boundary can mimic an impenetrable cell membrane, the reaction container's surface or be an effective virtual frontier of the “zone of influence” of the target molecule, separating it from other remotely located target molecules.

Assuming that the domain has a spherical shape and placing the target at the origin of this domain renders the model exactly solvable. We note that although such a geometrical setup is simplified as compared with realistic situations (e.g., the target site is not necessarily located at the centre of the domain^{28,29} or may be attached to some structure which partially screens it^{35,36}), this model captures explicitly two essential ingredients of the reaction process: the diffusive search for the target site and its finite intrinsic reactivity. Importantly, the fact that the model is exactly solvable, permits us to unveil some generic features of the full RTD without resorting to any approximation.

The probability density function $H(r, t)$ of the reaction time t for a particle released a radial distance $r-\rho$ away from the spherical target of radius ρ is calculated using standard tools:^{27,37,38} one first finds the survival probability $S(r, t)$ of a diffusing particle in a radially symmetric situation subject to the zero-current boundary condition on the outer boundary of the domain, and the “radiation”, or partially-reflecting boundary condition^{1-3,39}

$$D \frac{\partial S(r, t)}{\partial r} \Big|_{r=\rho} = \kappa S(\rho, t), \quad (2)$$

imposed on the surface of the target site. The proportionality factor κ in Eq. (2) is an intrinsic rate constant (of dimension length/time) whose value shows how readily the particle reacts with the target site upon encounter. When $\kappa=0$ no reaction occurs, while the limit $\kappa=\infty$ corresponds to a perfect reaction, when a particle reacts with the target site upon a first encounter. These limiting cases therefore correspond to perfectly reflecting or absorbing boundaries, respectively. The RTD $H(r, t)$ is obtained as the negative derivative of $S(r, t)$ and is valid for arbitrary values of the system parameters. Details of these calculations are presented in the beginning of the Methods section.

Structure of the full distribution of reaction times. The typical shapes of the reaction time density $H(r, t)$ are shown in Fig. 1 for two different release radii r and different values of the dimensionless reactivity $\kappa R/D$. Note that the parameter $\kappa R/D$ represents a combined effect of two factors: based on the definition of the standard chemical constant $K_{\text{on}} = 4\pi\rho^2\kappa$ for a forward reaction and the definition of the so-called Smoluchowski constant $K_S =$

$4\pi D\rho$ we see that $\kappa R/D = (K_{\text{on}}/K_S)(R/\rho)$ and, hence, this is the ratio of the chemical rate and the Smoluchowski rate constant, multiplied by the ratio of the sizes of the domain and of the target site.

We notice that $H(r, t)$ has a much richer structure than the previously proposed simple form in Eq. (1). The RTD consists of four distinct time domains seen in Figs. 1–3: first, a sharp exponential cut-off at short reaction times terminating at the most probable time t_{mp} ; second, a region spanning from the most probable reaction time to the crossover time t_c in which $H(r, t)$ shows a slow power-law decrease; third, an extended plateau region beyond t_c which stretches up to the mean reaction time t_{mean} ; and fourth, an ultimate long-time exponential cut-off. The shape of the RTD for varying reactivities highlighting the geometry-controlled Lévy–Smirnov hump and the reaction-controlled plateau region is our central result. In order to get a deeper understanding of the time scales involved in the reaction process, we also introduce and analyse in the Methods section the forms of two complementary characteristic times: the harmonic mean reaction time $t_{\text{harm}} = 1/\langle 1/t \rangle$ and the typical reaction time $t_{\text{typ}} = t_0 \exp(\langle \ln(t/t_0) \rangle)$, where the angular brackets denote averaging with respect to the RTD depicted in Figs. 1 and 2, and t_0 is an arbitrary time scale. Since the logarithm is a slowly varying function, its average value is dominated by the most frequent values of t , while anomalously large/small values corresponding to rare events provide a negligible contribution. Such an averaged value is widely used to estimate a typical behaviour in diverse situations^{40,41}.

Three characteristic time scales. The most probable reaction time, corresponding to the very pronounced maximum, can be

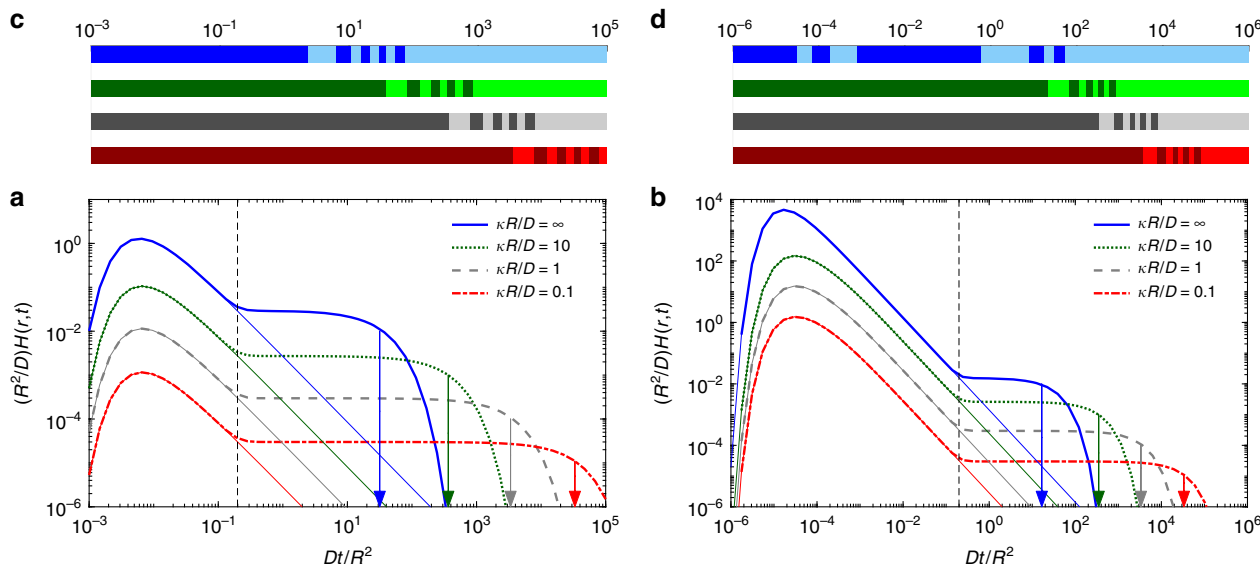


Fig. 1 Reaction control. Reaction time density $H(r, t)$ for a reaction on an inner target of radius $\rho/R = 0.01$, with starting point **a** $r/R = 0.2$ and **b** $r/R = 0.02$ for four progressively decreasing (from top to bottom) values of the dimensionless reactivity $\kappa' = \kappa R/D$ indicated in the plot. Note that κ' includes R and D such that smaller values of κ' can also be achieved at a fixed κ upon lowering R or by increasing the values of D . The coloured vertical arrows indicate the mean reaction times for these cases. The vertical black dashed line indicates the crossover time $t_c = 2(R - \rho)^2 / (D\pi^2)$ above which the contribution of higher order Laplacian eigenmodes become negligible. This characteristic time marks the end of the hump-like region (Lévy–Smirnov region specific to an unbounded system, see below and the Methods section for more details) and indicates the crossover to a plateau region with equiprobable realisations of the reaction times. This plateau region spans a considerable window of reaction times, especially for lower reactivity values. Thin coloured lines show the reaction time density $H_\infty(r, t)$ from Eq. (6) for the unbounded case ($R \rightarrow \infty$). Length and time units are fixed by setting $R = 1$ and $R^2/D = 1$. Note the extremely broad range of relevant reaction times (the horizontal axis) spanning over 12 orders of magnitude for the panel **b**. Coloured bar-codes **c**, **d** indicate the cumulative depths corresponding to four considered values of κ' in decreasing order from top to bottom. Each bar-code is split into ten regions of alternating brightness, representing ten 10%-quantiles of the distribution (e.g., the first dark blue region of the top bar-code in panel **c** indicates that 10% of reaction events occur till $Dt/R^2 \simeq 1$)

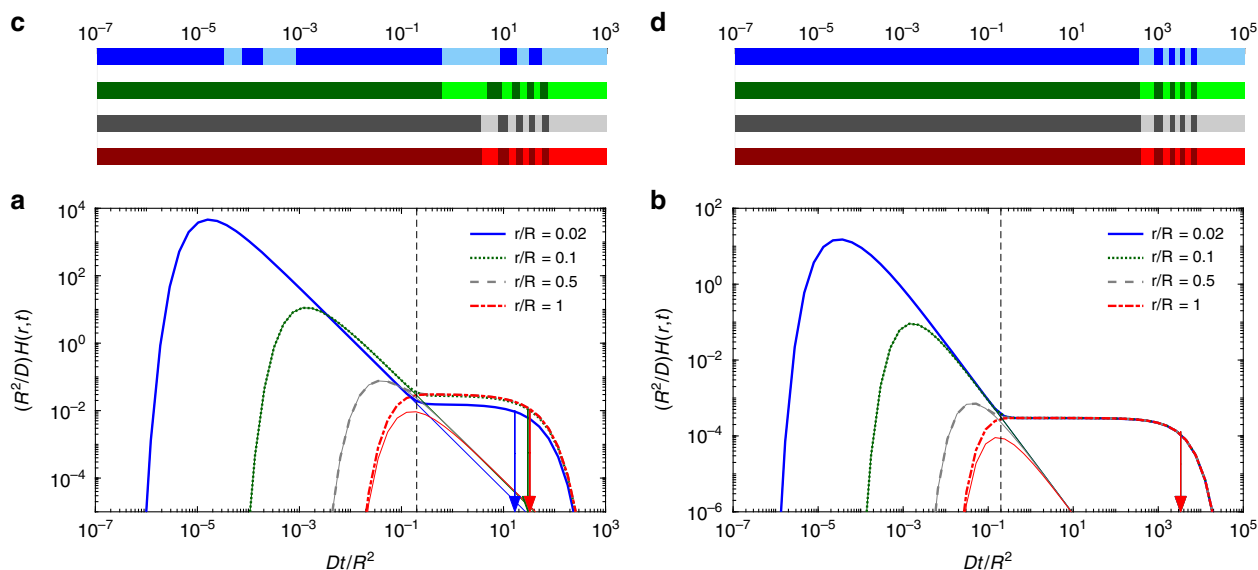


Fig. 2 Geometry control. Reaction time density $H(r, t)$ for a reaction on an inner target of radius $\rho/R = 0.01$, for the different initial radii r indicated in the panels (r increasing from top to bottom). The values of the reactivity are **a** $\kappa R/D = \infty$ (perfectly reactive) and **b** $\kappa R/D = 1$ (partially reactive). The coloured vertical arrows indicate the mean reaction times for these cases (note that some arrows coincide). The vertical black dashed line indicates the crossover time $t_c = 2(R - \rho)^2 / (D\pi^2)$ from the hump-like Lévy-Smirnov region to a plateau-like one. Thin coloured lines show the reaction time density $H_\infty(r, t)$ from Eq. (6) for the unbounded case ($R \rightarrow \infty$). The length and time units are fixed by setting $R = 1$ and $R^2/D = 1$. Clearly the positions of the most probable reaction times are geometry-controlled by the initial distance to the target. Not surprisingly, for the largest initial distance the solution for the unbounded case underestimates the RTD hump. Note the extremely broad range of relevant reaction times (horizontal axis) spanning over 12 orders of magnitude in panel **b**. Coloured bar-codes **c**, **d** indicate the cumulative depths corresponding to four considered values of r/R in increasing order from top to bottom. Each bar-code is split into ten regions of alternating brightness, representing ten 10%-quantiles of the distribution. In spite of distinctions in the probability densities in panel **b**, the corresponding cumulative distributions are close to each other and result in very similar reaction depths

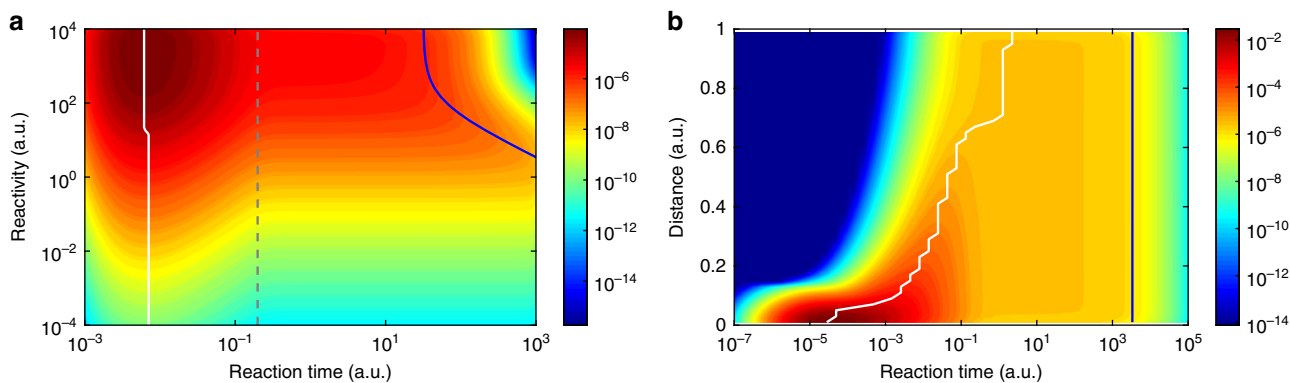


Fig. 3 Reaction versus geometry control. Impact of the finite reactivity (reaction control, **a**) and of the distance to the target (geometry control, **b**) onto the reaction time density shown as a “heatmap”, in which the value of the reaction time density (in arbitrary units) is determined by the colour code. Blue and white lines respectively show the mean and the most probable reaction times that differ by orders of magnitude. The grey vertical line indicates the crossover time t_c that does depend neither on reactivity, nor on distance. **a** When the reactivity κ decreases (with $r/R = 0.2$ being fixed), the distribution becomes much broader and extends towards longer reaction times. **b** When the distance to the target decreases (with $\kappa R/D = 1$ fixed), the most probable reaction time shifts to the left, whereas the mean reaction time remains constant

calculated explicitly (see the Methods section) and has the approximate form

$$t_{\text{mp}} \approx (r - \rho)^2 / (6D). \quad (3)$$

Interestingly, this simple estimate, which depends only on the diffusion coefficient and the initial distance to the target site, appears to be very robust: t_{mp} indeed shows very little variation with the reactivity κ , as one may infer from Figs. 1 and 3. In the Methods section, we show that when κ decreases from infinity to

zero, the value of t_{mp} varies only by a factor of 3. This characteristic time is always strongly skewed towards the left tail of the distribution, that is, to short reaction times: t_{mp} in fact corresponds to particles moving relatively directly from their starting point to the target followed by an immediate reaction and thus generalises the concept of direct, purely geometry-controlled trajectories²² to systems with reaction control. Note that expression (3) is different from the diffusion-controlled additive contribution proportional to $1/D$ in the mean reaction time (5).

The second characteristic time scale is the crossover time t_c from the hump-like Lévy-Smirnov region specific to an

unbounded system, to the plateau region. Hence, t_c can be interpreted as the time at which a molecule starts to feel the confinement. This can be nicely discerned from comparison with the density $H_\infty(r, t)$ for the unbounded case (Fig. 2). Thus, reaction times beyond t_c correspond to indirect trajectories²². From the result

$$t_c \approx 2(R - \rho)^2 / (\pi^2 D) \quad (4)$$

obtained in the Methods section, we see that t_c is independent of the starting point and of the reactivity κ , being entirely dominated by the diffusivity and the difference between the sizes of the domain R and of the target. Writing $t_{\text{mp}}/t_c = \pi^2(r - \rho)^2/[12(R - \rho)^2]$, one realises that the crossover time can be comparable with the most probable time (such that the hump-like region shrinks), but may also become much larger than the latter when r is close to ρ , as it happens, e.g., when proteins are produced in a close vicinity of a first gene activated at $t = 0$. In this case, of course, the hump-like region will be most pronounced (Fig. 2).

Finally, the onset of the right exponential shoulder at long reaction times coincides with the mean reaction time, as indicated by the arrows in Figs. 1 and 2. The latter is obtained from the Laplace transformed distribution (see the Methods section) and is given by the exact formula

$$t_{\text{mean}} = \frac{(r - \rho)(2R^3 - \rho r(r + \rho))}{6D\rho} + \frac{R^3 - \rho^3}{3\kappa\rho^2}, \quad (5)$$

which can be thought of as an analogue of the celebrated Collins–Kimball relation for the apparent reaction rate¹³. The first term in Eq. (5) is the standard MFPT to a perfectly reactive target and corresponds to the classical notion of diffusion-controlled rate. The additional contribution to t_{mean} proportional to κ^{-1} accounts for the imperfect reaction with finite reactivity, independent of the particle's starting point. When t_{mean} is a unique time scale characterising exhaustively well the reaction kinetics, as it happens for reactions with sufficiently high concentrations of reactants, one can indeed distinguish between diffusion or kinetic control. In contradiction, for reactions with nanomolar concentrations of reactive species, the other time scales t_{mp} and t_c are equally important and no clear-cut separation between diffusion and kinetic control can be made. In the Methods section, we also present an explicit exact expression for the variance of the first reaction time, which permits us to determine the coefficient of variation of the RTD and hence, to quantify its broadness.

Geometry versus reaction control. We emphasise that even for perfect reactions, for which $\kappa = \infty$, the mean reaction time is orders of magnitude longer than the most probable reaction time. For imperfect reactions (finite κ values) the mean reaction time becomes even longer, and diverges as $1/\kappa$ when $\kappa \rightarrow 0$. The fact that the most probable reaction time is very weakly dependent on κ renders the difference between the most probable and the mean reaction times so much more severe for finite κ . Another remarkable and so far unnoticed feature is that a pronounced plateau develops beyond t_c , reflecting an emergent regime of reaction-control. This plateau exists even for $\kappa = \infty$ (Fig. 1) and becomes increasingly longer with decreasing reactivity κ , implying that over several decades the values of the reaction time become equally probable. Mathematically speaking this plateau appears due to the fact that the smallest eigenvalue of the boundary value problem—the only eigenvalue with an appreciable dependence on κ —disentangles from the remaining eigenvalues. This point is discussed in more detail in the Methods

section. Physically, the emergence of the plateau implies that the first passage process to the reaction event becomes even more defocused with decreasing κ , i.e., that the spread of possible reaction times increases significantly. The long spread of reaction times within this plateau region is a consequence of geometrically defocused trajectories exploring the boundary of the reaction volume reinforced by the necessary multiple collisions with the target before a final reaction event due to the reaction-control with finite reactivity. An important consequence of the existence of the extended plateau region is that all positive moments of $H(r, t)$, not only the mean reaction time, will be dominated by integration over this region. In other words, the resulting RTD is a concerted effect of geometry-control and reaction-control.

In Fig. 2, we analyse the effect of the initial distance to the surface of the target site for both perfect and imperfect reactions. The exponential shoulder at long reaction times almost coincides for all cases, especially when the reactivity is finite. This part of the reaction time distribution is dominated by trajectories that equilibrate in the volume before eventual reaction (indirect trajectories²²). In contrast, we see a strong variation of the most probable reaction time. The exponential cut-off at short reaction times and the position of the maximum of the distribution is geometry-controlled, as can be anticipated from the Lévy–Smirnov form for the unbounded problem (see the Methods section): direct trajectories from the initial position to the target need a minimum travel time. For increasing initial distance, the most probable reaction time thus moves to longer times and the relative contribution of the geometry-controlled fraction of direct trajectories becomes less relevant: instead the particles almost fully equilibrate in the confined volume until they finally react with the target. This reaction-control effect is accentuated for decreasing reactivity. We stress that for biological applications, both cases are relevant: shorter initial distances, for instance, are involved when proteins are produced around a first gene activated at time $t = 0$ and these proteins then need to move to a close-by second gene, here represented by the inner target. This scenario is very similar to the one discussed in reference¹⁹ as an example for the rapid search hypothesis¹⁸. Longer initial distances are relevant when a molecular signal passes the cellular membrane or is produced around a cytoplasmic plasmid, and when these molecules then need to diffuse to the nucleoid region in a bacterial cell or pass the nuclear membrane in an eukaryotic cell. Figure 3 summarises the effects of the finite reactivity and of the distance to the target onto the reaction time distribution in the form of a “heat map”.

Short- and long-time behaviour. We now turn to the discussion of the short- and long-time tails of $H(r, t)$. The long-time behaviour of the density $H(r, t)$ is determined by the smallest eigenvalue λ_0 of the Laplace operator. For the spherical domain, one can accurately compute this eigenvalue by solving a trigonometric equation (see the Methods section). When both the target and its reactivity are small one gets $\lambda_0 \approx \kappa S_\rho / (DV)$, where the surface area $S_\rho = 4\pi\rho^2$ of the target and the volume of the domain $V \approx 4\pi R^3/3$ are introduced. According to Eq. (5), in this limit $t_{\text{mean}} \approx 1/(D\lambda_0)$, i.e., the mean reaction time is dominated by multiple returns to the target until the reaction occurs. As the target shrinks (ρ vanishes), the smallest eigenvalue tends to zero. In turn, the other eigenvalues λ_n , corresponding to rotation-invariant eigenfunctions of the Laplace operator in the spherical domain, are bounded from below: $\lambda_n > \pi^2 n^2 / R^2$ for $n = 1, 2, \dots$. As a consequence, there is an intermediate range of times, $1/(D\lambda_1) \ll t \ll 1/(D\lambda_0)$, for which the contribution of all higher-order eigenmodes vanishes, that is, $e^{-Dt\lambda_n} \ll 1$, whereas

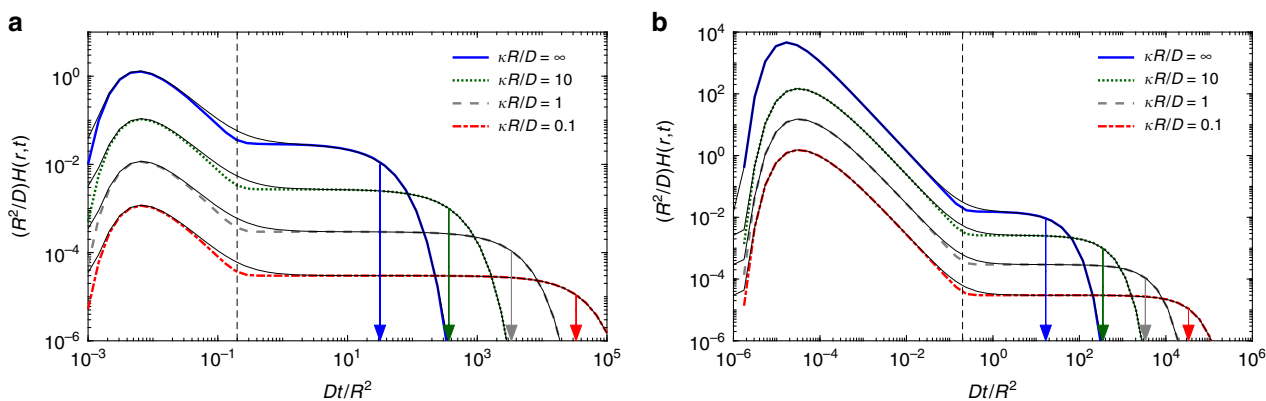


Fig. 4 Explicit approximation for the reaction time density $H(r, t)$. It is evaluated for a reaction with an inner target of radius $\rho/R = 0.01$ with starting point **a** $r/R = 0.2$ and **b** $r/R = 0.02$, and four values of the dimensionless reactivity $\kappa' = \kappa R/D$ (decreasing from top to bottom). The coloured vertical arrows indicate the respective mean reaction time. The black vertical dashed line shows the crossover time $t_c = 2(R - \rho)^2/(D\pi^2)$ above which the contribution of higher order Laplacian eigenmodes become small. Thin black lines show the approximation (8) of the RTD which very nicely captures the main features of the exact density. Length and time units are fixed by setting $R = 1$ and $R^2/D = 1$

the contribution of the lowest eigenmode is almost constant in time, $e^{-Dt\lambda_0} \approx 1$. This is precisely the reason why the intermediate, plateau-like region emerges, see Fig. 1. Note that this region protrudes over an increasing range of time scales when either the reactivity κ or the target radius ρ decrease, or both. Note also that this intermediate regime corresponds approximately to an exponential law which is often evoked in the context of the first passage statistics to small targets, see, for instance, references^{28,42,43}.

While the smallest eigenvalue determines the plateau and the ultimate exponential cut-off, the short-time behaviour of the reaction time density $H(r, t)$ is determined by other eigenmodes. Since the limit of a small target ($\rho \ll R$) can alternatively be seen as the limit of large domain size, one can use the density $H_\infty(r, t)$ for diffusion in the exterior of a target, which was first derived by Collins and Kimball¹³,

$$H_\infty(r, t) = \frac{\kappa}{r} \exp\left(-\frac{(r-\rho)^2}{4Dt}\right) \left\{ \frac{\rho}{\sqrt{\pi Dt}} - \left(1 + \frac{\kappa\rho}{D}\right) \operatorname{erfcx}\left(\frac{r-\rho}{\sqrt{4Dt}} + \left(1 + \frac{\kappa\rho}{D}\right) \frac{\sqrt{Dt}}{\rho}\right) \right\}, \quad (6)$$

where $\operatorname{erfcx}(x) = e^{x^2} \operatorname{erfc}(x)$ is the scaled complementary error function (its derivation is reproduced in the Methods section). As demonstrated in Fig. 1, Eq. (6) fully captures the geometry-controlled part of the reaction time distribution. In the limit of a perfectly absorbing target, $\kappa \rightarrow \infty$, this expression reduces to

$$H_\infty(r, t) = \frac{\rho}{r} \frac{r-\rho}{\sqrt{4\pi Dt^3}} \exp\left(-\frac{(r-\rho)^2}{4Dt}\right), \quad (7)$$

whose normalisation $\rho/r \leq 1$ reflects the transient nature of diffusion in three dimensions. One can easily check that the maximum of this Lévy–Smirnov-type density is given precisely by Eq. (3), as intuitively expected.

Approximate form of the full distribution. Combining the short- and long-time contributions, we arrive at the following approximate formula for the reaction time density

$$H(r, t) \approx H_\infty(r, t) + (1 - q) \frac{e^{-t/t_{\text{mean}}}}{t_{\text{mean}}}, \quad (8)$$

where $t_{\text{mean}} \approx 1/(D\lambda_0)$ and

$$q = \int_0^\infty dt H_\infty(r, t) = \frac{\rho/r}{1 + D/(\kappa\rho)} < 1 \quad (9)$$

is the hitting probability of the target. The correct normalisation of $H(r, t)$ is ensured by the prefactor in front of the second term. Result (8) is substantially more general than the simple form (1) suggested in ref. 28. The form (8) not only extends expression (1) to the partially-reactive case, i.e., for arbitrary finite values of κ , but also emphasises and provides an explicit form for the contribution from the hump-like region around t_{mp} , which is most relevant for reactions in which the molecule starts close to the target.

Figure 4 illustrates the quality of this approximation, showing that it becomes most accurate when the target radius ρ or reactivity κ are small. One observes that it accurately captures both the maximum, the plateau, and the exponential cut-off of the reaction time distribution. In turn, the transition between the maximum and the plateau region is less sharp than in the exact form. A minor inaccuracy of the approximation (8) is that it reaches a constant—set by the second term—in the short-time limit while the exact distribution vanishes as $t \rightarrow 0$. This feature can be simply removed by multiplying the second term by a Heaviside step function $\Theta(t - t_c)$ and re-evaluating the normalisation constant. But even in the present form approximation (8) provides a remarkably good insight into the behaviour of the first passage dynamics and can thus be used as an efficient and easy-to-handle fit formula for data analysis or for explicit analytical derivations of follow-up processes.

Reaction depth. Lastly, we point out that the contributions of the four different regimes separated by the time scales t_{mp} , t_c , and t_{mean} can be further quantified by the corresponding reaction depths defining which fraction of trajectories reacted up to a given time. We thus focus now on the cumulative distribution function of reaction times

$$F_r(t) = \int_0^t dt' H(r, t') = 1 - S(r, t), \quad (10)$$

with the evident property $F_r(\infty) = 1$ in a bounded domain in which $H(r, t)$ is normalised, and thus shows explicitly which fraction of trajectories have reacted up to time t . The reaction

Table 1 Impact of the target reactivity and proximity onto the reaction depth

r/R	region	$\kappa' = \infty$	$\kappa' = 10$	$\kappa' = 1$	$\kappa' = 0.1$
0.2	Hump-like	3.8	0.34	0.04	0.004
	Plateau-like	59.4	62.9	63.2	63.2
	Exponential tail	36.8	36.8	36.8	36.8
0.02	Hump-like	49.4	4.4	0.5	0.05
	Plateau-like	20.0	58.8	62.7	63.15
	Exponential tail	30.6	36.8	36.8	36.8

Relative weights (in percents) of three characteristic regions of the reaction time density for $\rho/R = 0.01$: the hump-like region around the most probable reaction time t_{mp} , extending from 0 till $t_c = 2(R-\rho)^2/(\kappa^2 D)$ (and thus merging two subregions discussed in the text: the exponential tail left to t_{mp} and the power-law decay right to t_{mp}); the plateau-like region stretching from t_c to the mean reaction time t_{mean} ; and the exponential tail which persists beyond $t = t_{mean}$. Two starting points r/R and four values of dimensionless reactivity $\kappa' = \kappa R/D$ are used, corresponding to Fig. 1.

depth is illustrated in the Methods section. Table 1 summarises the values of the reaction depths of the three characteristic regions of the RTD: the hump-like region around t_{mp} , the plateau region, and the exponential tail. We realise that for $r/R = 0.2$ the least amount of the reaction events happens within the hump-like region: it is of order of just 4% for perfect reactions, and this fraction rapidly diminishes upon a decrease of κ . In turn, a much larger amount of the reaction events is collected within the final exponential region. It is typically of order of almost 37%, independently of the value of κ , meaning that for such a value of the ratio r/R roughly one third of all realisations remain unreacted at time $t = t_{mean}$. However, most of realisations of the reaction events occur within the plateau-like regime—it amounts to roughly 59% for perfect reactions, and becomes even bigger for smaller values of κ . The situation becomes different for a smaller release radius: $r/R = 0.02$. Here, for perfect reactions the majority of trajectories (49% such that t_c is close to the median time) react within the hump-like region, while the plateau region and the final exponential tail contribute only 20 and 30%, respectively. Upon lowering κ , the hump-like region is no longer representative, and more reaction events take place during the exponential tail (~37%) and the plateau-like regions (~63%), respectively. In conclusion, the plateau region appears to be the most important part of the RTD, which contributes most to the overall number of reaction events, except for the case $r/R \ll 1$ and $\kappa R/D \gg 1$, for which the hump-like region becomes the dominant one. Concurrently, this plateau is the region of the strongest defocusing effect, in particular for increased reaction-control.

Discussion

Many molecular signalling processes in living biological cells run off at minute concentrations. Similarly in vitro experiments tracking the motion of colloidal particles employ only few particles. Individual first passage events in such situations are defocused, that is, possible reaction times are spread over a vast range comprising orders of magnitude. In particular, this implies that any pair of reaction events will be characterised by highly disparate reaction times. The quantitative description of the reaction time to a target in this scenario therefore cannot simply be based on the mean reaction time. As we showed, the resulting broad distribution of reaction times is due to a conspiracy between geometry-control and reaction-control effects which cannot be disentangled.

We analysed this phenomenon in detail for a generic spherical geometry, concentrating on several main features. (i) The reaction time density consists of four regions with distinct asymptotic behaviour. (ii) These time regions are separated by three characteristic time scales, which means that there is no unique time

scale characterising the kinetic behaviour exhaustively well and the reaction times are defocused. In consequence, the textbook notions of diffusion versus kinetic control, which are appropriate for reactions operating at abundant concentrations, are not applicable in our case. We explicitly determined these times scales and also the associated reaction depths. (iii) A finite reactivity broadens an intermediate regime characterised by an extended plateau region. We showed that the plateau emerges due to a time scale separation of the lowest and the next eigenvalues of the diffusion-controlling Laplace operator. The fundamental parameter that we found to quantify this intermediate regime is the reaction-control represented by the dimensionless reactivity $\kappa R/D$. A majority of the reaction events occur within this region, except for the case $r/R \ll 1$ and $\kappa R/D \gg 1$. In turn, for perfect reactions with a reactant starting very close to the target site the most important part of the RTD is the hump-like region which contributes with almost 50% of the reaction events. (iv) The geometry control of the initial particle-to-target distance strongly affects the position and the amplitude of the maximum of the reaction time distribution and thus the most probable reaction time. (v) We came up with a simple and thus practical approximate formula for the full reaction time distribution. In particular, we demonstrated that this approximation captures both the most probable and mean reaction times. While the derivation relied on the rotation symmetry of the considered geometric domain, this approximation is expected to be valid in more complex confinements, as long as the target site is far enough from the surrounding outer boundary. Our main conclusion is that reaction-control with finite reactivity leads to even stronger reaction time defocusing, stressing the necessity to know the full RTD. This conclusion will serve as a benchmark for the behaviour in geometrically more complex situations²⁹ when, e.g., the target site is on the wall or bound to some geometrical structure within the domain, and a fully analytical solution is impossible.

Methods

Exact distribution of reaction times. We consider a diffusion process in a three-dimensional domain $\Omega = \{\mathbf{x} \in \mathbb{R}^3 : \rho < \|\mathbf{x}\| < R\}$ between two concentric spheres—a small target and a bounding surface of radii ρ and R , respectively. Although the solution of the underlying diffusion problem is well known^{27,38}, we rederive it here for completeness and to highlight several practical points discussed in the main text. In fact, the Laplace transformed probability density function $\tilde{H}(\mathbf{x}, p)$ satisfies the modified Helmholtz equation

$$(p - D\Delta)\tilde{H}(\mathbf{x}, p) = 0 \quad (\mathbf{x} \in \Omega), \quad (11)$$

subject to the boundary conditions

$$(\partial_n \tilde{H}(\mathbf{x}, p))|_{\|\mathbf{x}\|=R} = 0, \quad (12a)$$

$$\left(\frac{D}{\kappa} \partial_n \tilde{H}(\mathbf{x}, p) + \tilde{H}(\mathbf{x}, p)\right)|_{\|\mathbf{x}\|=\rho} = 1. \quad (12b)$$

Here, Δ is the Laplace operator, D is the diffusion coefficient, κ is the intrinsic reactivity, and ∂_n is the normal derivative directed outward from the domain Ω .

The rotational symmetry of the domain reduces the partial differential Eq. (11) to an ordinary differential equation with respect to the radial coordinate r ,

$$\begin{aligned} \tilde{H}''(r, p) + \frac{2}{r} \tilde{H}'(r, p) - \frac{p}{D} \tilde{H}(r, p) &= 0, \\ \tilde{H}'(R, p) &= 0, \end{aligned} \quad (13)$$

$$\left(\tilde{H}(r, p) - \frac{D}{\kappa} \tilde{H}'(r, p)\right)_{r=\rho} = 1,$$

where primes denote derivatives with respect to r . The solution of this equation is

$$\tilde{H}(r, p) = \frac{g(r)}{g(\rho) - g'(\rho) \frac{D}{\kappa}}, \quad (14)$$

where

$$g(r) = \frac{R\sqrt{\rho/D}\cosh\xi - \sinh\xi}{r\sqrt{\rho/D}}, \quad (15)$$

with $\xi = (R-r)\sqrt{\rho/D}$. It follows that

$$g'(r) = \frac{(1-R\rho/D)\sinh\xi - \xi\cosh\xi}{r^2\sqrt{\rho/D}}. \quad (16)$$

The mean reaction time is obtained from the Laplace-transformed density as

$$t_{\text{mean}} = -\lim_{p \rightarrow 0} \frac{\partial}{\partial p} \tilde{H}(r, p), \quad (17)$$

from which Eq. (5) follows.

In the limit $R \rightarrow \infty$, Eqs (14–16) yield

$$\tilde{H}_{\infty}(r, p) = \frac{(\rho/r)e^{-(r-\rho)\sqrt{\rho/D}}}{1 + (1 + \rho\sqrt{\rho/D})D/(\kappa\rho)}. \quad (18)$$

Due to the transient character of three-dimensional diffusion, the related distribution is not normalised to unity, but $\tilde{H}_{\infty}(r, p=0) = (\rho/r)/(1 + D/(\kappa\rho)) < 1$ is the probability of reacting with the target before escaping to infinity. The inverse Laplace transform of Eq. (18) yields Eq. (6). Using the relation $\tilde{S}_{\infty}(r, p) = (1 - \tilde{H}_{\infty}(r, p))/p$ and Eq. (18), one can also compute the survival probability $S_{\infty}(r, t)$ in the time domain

$$S_{\infty}(r, t) = 1 - \frac{\rho \exp\left(-\frac{(r-\rho)^2}{4Dt}\right)}{r(1 + D/(\kappa\rho))} \left\{ \operatorname{erfcx}\left(\frac{r-\rho}{\sqrt{4Dt}}\right) - \operatorname{erfcx}\left(\frac{r-\rho}{\sqrt{4Dt}} + \left(1 + \frac{\kappa\rho}{D}\right)\frac{\sqrt{Dt}}{\rho}\right) \right\}. \quad (19)$$

Now we come back to a bounded case with $R < \infty$. The Laplace inversion of Eq. (14) can be performed by identifying the poles of the function $\tilde{H}(r, p)$ in the complex plane $p \in \mathbb{C}$, that is, by finding the zeros of the function

$$F(p) = g(p) - \frac{D}{\kappa} g'(p). \quad (20)$$

For convenience, we introduce dimensionless Laplace variable $s = (R-\rho)^2 p/D$, so that

$$F(p) = \frac{1}{\rho^2 \sqrt{s}} \left((\rho R + \mu(R-\rho)^2) \sqrt{s} \operatorname{cosh}\sqrt{s} - (\rho(R-\rho) + \mu(R-\rho)^2 - \mu R \rho s) \sinh\sqrt{s} \right), \quad (21)$$

where we defined the dimensionless “dilatortiness” parameter μ as

$$\mu = \frac{D}{\kappa(R-\rho)}. \quad (22)$$

The perfectly reactive target with $\kappa = \infty$ corresponds to $\mu = 0$. In other words, for high reactivity κ the value of the dilatortiness μ is small and reactions occur more likely on first encounter, and vice versa. Note that a fully reflecting target with $\kappa = 0$ is excluded from our analysis because the reaction time would be infinite. In other words, we always consider $0 \leq \mu < \infty$.

The solutions of the equation $F(p) = 0$ lie on the negative real axis. Setting $s = -\alpha^2$, one gets the trigonometric equation

$$\tan \alpha = \frac{\alpha(\rho R + \mu(R-\rho)^2)}{\rho(R-\rho) + \mu(R-\rho)^2 + \mu R \rho \alpha^2}. \quad (23)$$

This equation has infinitely many positive solutions that we denote as α_n , with $n = 0, 1, 2, \dots$. Since the function on the right-hand side has the slope

$\frac{\rho R + \mu(R-\rho)^2}{\rho(R-\rho) + \mu(R-\rho)^2} > 1$ near $\alpha = 0$, the smallest solution α_0 lies in the interval $(0, \pi/2)$.

More generally, the n th solution lies in the interval $(\pi n, \pi(n+1/2))$ and tends, for any fixed κ , to the left boundary of the interval as $n \rightarrow \infty$. Note that $\alpha = 0$ (or $p = 0$) is not a pole of the function $\tilde{H}(r, p)$.

Once the poles are identified, we determine the residues by taking the derivative of $F(p)$ at the poles. Applying the theorem of residues to compute the inverse Laplace transform, we finally deduce the exact expression for the probability density $H(r, t)$ of the reaction time for a particle starting at a distance $r-\rho$ from the

target,

$$H(r, t) = \sum_{n=0}^{\infty} u_n(r) e^{-Dt\lambda_n}, \quad (24)$$

with

$$\lambda_n = \alpha_n^2 / (R-\rho)^2, \quad (25)$$

$$u_n(r) = c_n \frac{D}{(R-\rho)^2} \times \frac{R\alpha_n \cos\left(\alpha_n \frac{R-r}{R-\rho}\right) - (R-\rho) \sin\left(\alpha_n \frac{R-r}{R-\rho}\right)}{r\alpha_n}, \quad (26)$$

where the expansion coefficients c_n are given explicitly by the residues as

$$c_n = \frac{2\rho^2 \alpha_n^2}{(\rho R + \mu(R^2 + \rho^2))\alpha_n \sin \alpha_n + \rho(\mu R \alpha_n^2 - \rho) \cos \alpha_n}. \quad (27)$$

Long-time behaviour of the RTD. When either the target radius ρ is small or the dilatortiness parameter μ is large, the slope of the right-hand side of Eq. (23) is close to unity and thus the smallest eigenvalue α_0 is close to zero. Expanding both sides of Eq. (23) into Taylor series one finds the first-order approximation

$$\alpha_0 \simeq \frac{\rho}{\sqrt{\rho(R-\rho) + \mu(R-\rho)^2}} \times \left(\frac{1}{3} + \mu R \rho \frac{\rho R + \mu(R-\rho)^2}{(\rho(R-\rho) + \mu(R-\rho)^2)^2} \right)^{-1/2} + \dots \quad (28)$$

In particular, for small target radius, $\rho \rightarrow 0$, at fixed dilatortiness μ , we see that $\alpha_0 \simeq \sqrt{3}(\rho/R)\mu^{-1/2}$. In turn, when $\mu \rightarrow \infty$ with fixed ρ ,

$$\alpha_0 \simeq \frac{\sqrt{3}\rho}{\sqrt{R^2 + R\rho + \rho^2}} \mu^{-1/2}. \quad (29)$$

In both cases, α_0 is proportional to ρ and inversely proportional to $\sqrt{\mu}$. As a consequence, the term with the slowest decay time behaves as

$$\lambda_0 \simeq \frac{3\kappa\rho^2}{D(R-\rho)(R^2 + R\rho + \rho^2)} \simeq \frac{3\kappa\rho^2}{DR^3} \simeq \frac{\kappa S_p}{DV}, \quad (30)$$

where in the intermediate approximation we ignored terms of order ρ/R and higher, and we introduced the surface area $S_p = 4\pi\rho^2$ of the target and the volume of the domain $V \simeq 4\pi R^3/3$.

We also note that the approximation $c_0 \simeq 3(\rho/R)^2/(\mu + 3\rho/(2R))$ holds for $\rho \ll R$, and thus $c_0/\alpha_0^2 \simeq 1/(1 + 3\rho/(2\mu R))$, i.e., it is close to unity as long as the dilatortiness μ is not too small. Therefore the survival probability can be accurately approximated as $S(r, t) \simeq \exp(-Dt\alpha_0^2/R^2)$ for intermediate and large times. In this case the median reaction time becomes

$$t_{\text{median}} \simeq \frac{R^2 \ln 2}{D\alpha_0^2} \simeq \frac{\mu R^4 \ln 2}{3D\rho^2} \simeq \frac{R^3 \ln 2}{3\kappa\rho^2}, \quad (31)$$

from which the relation $t_{\text{median}} \simeq t_{\text{mean}} \ln 2$ follows. This median value is close to the mean reaction time, in which the limit $\rho \ll R$ has the dominant behaviour as $R^3/(3\kappa\rho^2)$ according to Eq. (5). In turn, the most probable reaction time, which is determined by the higher-order eigenmodes, is orders of magnitude smaller. This behaviour is, however, only present for weakly reactive targets. In contrast, the median time for perfect reactions is usually close to the crossover time t_c , while t_{mean} is orders of magnitude larger.

Most probable reaction time. One may deduce from Fig. 1 that the region around the most probable reaction time is well described by the function in (6), which corresponds to the solution in the limit $R \rightarrow \infty$. Hence, the most probable reaction time t_{mp} can be obtained with a good accuracy by merely differentiating this function with respect to t and setting the result equal to zero:

$$t_{\text{mp}} = \frac{(r-\rho)^2}{6D} z^2, \quad (32)$$

where z is defined implicitly as the solution of the following, rather complicated transcendental equation

$$\beta^2 z^4 - 3(1 + \beta)z^2 + 9 - \sqrt{\pi/6}\beta^3 z^5 \operatorname{erfcx}\left(\frac{\sqrt{3/2}}{z} + \frac{\beta z}{\sqrt{6}}\right) = 0, \quad (33)$$

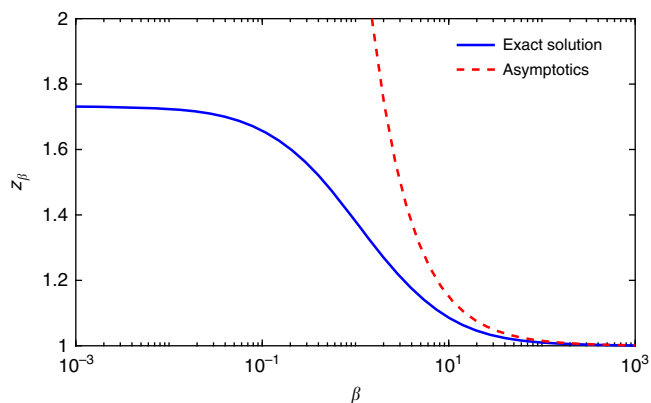


Fig. 5 Weak dependence of the most probable reaction time on reactivity. The numerical solution z_β of Eq. (33) as a function of β (solid line) and its large- β asymptotic behaviour (35) are shown by the dashed line

where $\text{erfcx}(x)$ is the scaled complementary error function, and

$$\beta = \frac{r-\rho}{\rho} \left(1 + \frac{\kappa\rho}{D}\right). \quad (34)$$

We denote the solution of this equation as z_β . When β tends to 0, a Taylor expansion of the left-hand side of (33) yields $z^2 - 9 + O(\beta)$, from which $z_0 = \sqrt{3}$. In the opposite limit $\beta \rightarrow \infty$, one uses the asymptotic behaviour of the function $\text{erfcx}(x)$ to get

$$z_\beta \simeq 1 + \frac{3}{2\beta} + O(\beta^{-2}). \quad (35)$$

With some technical efforts, one can prove that z_β is a monotonously decreasing function of β (see Fig. 5). We conclude that z_β is bounded between $\sqrt{3}$ and 1 so that the most probable time t_{mp} lies between $(r-\rho)^2/(6D)$ (for $\kappa\rho \gg 1$) and $(r-\rho)^2/(2D)$ (for $\kappa\rho \ll 1$). In other words, the most probable reaction time shows remarkably weak dependence on the reactivity κ , as illustrated by Fig. 5.

Moments of the reaction time. As we have already remarked in the main text, the positive moments of the RTD of an arbitrary order are dominated by the integration over the plateau-like region such that their values appear close to the onset of the crossover to the final region—the exponential decay of the RTD. The exact values of the positive moments of the random reaction time τ can be accessed directly by a mere differentiation of $\tilde{H}(r, p)$ with respect to the Laplace parameter p and subsequently taking the limit $p \rightarrow 0$:

$$\langle \tau^k \rangle = (-1)^k \lim_{p \rightarrow 0} \frac{\partial^k \tilde{H}(r, p)}{\partial p^k}. \quad (36)$$

For instance, a lengthy but straightforward calculation yields the exact formula for the variance of the reaction time:

$$\begin{aligned} \langle \tau^2 \rangle - \langle \tau \rangle^2 = & \frac{1}{90D^2 r^2 \rho^2} \{ 10r^2(R^3 - \rho^3)^2(D/\kappa)^2 \\ & + 4\rho r^2(5R^3 + 6R^2\rho + 3R\rho^2 + \rho^3)(R-\rho)^3(D/\kappa) \\ & + \rho^2(r-\rho)(2R^3(5R^3\rho + 5R^2r + 10r^2\rho^2 - 18R^2r\rho) \\ & - \rho^2 r^2(\rho+r)(r^2 + \rho^2)) \}, \end{aligned} \quad (37)$$

from which one also gets the coefficient of variation, $\gamma = \sqrt{\langle \tau^2 \rangle - \langle \tau \rangle^2} / \langle \tau \rangle$, which characterises fluctuations of the random reaction time τ around its mean, i.e., the effective broadness of the reaction time density. As compared with ref. 30, the expressions Eqs. (5) and (37) permit us to quantify the effect of both rate-controlling factors.

For a perfectly reactive target, the coefficient of variation diverges as the starting point r approaches ρ , in particular, one gets

$$\gamma^2 \simeq \frac{2\rho}{r-\rho} + O(1), \quad (38)$$

when the target is small or the confining domain is large ($\rho \ll R$). In turn, for a partially reactive target, the squared coefficient of variation is finite in the limit $r \rightarrow$

ρ and for a small target reads

$$\gamma^2 \simeq 1 + \frac{2\rho\kappa}{D}. \quad (39)$$

The coefficient of variation γ in Eqs (38) and (39) exceeds 1, allowing one to classify this distribution as broad, according to the standard terminology in statistics^{24–26}. In both cases, the asymptotic behaviour of γ does not depend on the size of the confining domain, R .

We turn next to the negative order moments of the RTD which are clearly dominated by the region close to the origin and hence, probe the left tail of the distribution. The computation of negative moments (with $\nu > 0$) involves integration:

$$\langle \tau^{-\nu} \rangle = \int_0^\infty dt t^{-\nu} H(r, t) = \frac{1}{\Gamma(\nu)} \int_0^\infty dp p^{\nu-1} \tilde{H}(r, p). \quad (40)$$

Although this integral is expressed in terms of the explicitly known Laplace transform $H(r, p)$ from Eq. (14), its analytical evaluation does not seem to be feasible.

In turn, the integral takes a more tractable form in the limit $R \rightarrow \infty$ corresponding to diffusion in the exterior of a partially reactive target of radius ρ . Due to the transient character of diffusion in three dimensions, the probability density $H_\infty(r, t)$ is not normalised to 1 as the molecule can escape to infinity. The integral of the density $H(r, t)$ yields thus the probability of reacting at the target:

$$q = \tilde{H}_\infty(r, p=0) = \frac{\rho/r}{1 + D/(\kappa\rho)}. \quad (41)$$

The negative order moments of the renormalised density $H_\infty(r, t)/q$ are

$$\langle \tau^{-\nu} \rangle_n = \frac{2}{\Gamma(\nu)} \left(\frac{D}{(r-\rho)^2} \right)^\nu \int_0^\infty dz z^{2\nu-1} \frac{e^{-z}}{1 + z/\beta}, \quad (42)$$

where β was defined in (34). In the limit $\kappa \rightarrow \infty$, one finds

$$\langle \tau^{-\nu} \rangle_n = \frac{2}{\Gamma(\nu)} \left(\frac{D}{(r-\rho)^2} \right)^\nu \Gamma(2\nu). \quad (43)$$

While the mean reaction time diverges for the exterior problem, the negative order moments are well-defined and can thus characterise the reaction process. In particular, the harmonic mean reaction time, defined as

$$t_{\text{harm}} = \frac{1}{\langle \tau^{-1} \rangle_n}, \quad (44)$$

is deduced from (42) for $\nu = 1$:

$$t_{\text{harm}} = \frac{(r-\rho)^2}{2D} \beta^{-1} (1 - \beta e^\beta \text{Ei}_1(\beta))^{-1}, \quad (45)$$

where $\text{Ei}_1(z) = \int_1^\infty dx e^{-zx}/x$ is the exponential integral. The dependence of the harmonic mean on the reactivity κ is fully captured via β . In the limit $\kappa \rightarrow \infty$, this mean approaches

$$t_{\text{harm}} = \frac{(r-\rho)^2}{2D}, \quad (46)$$

and is thus of the order of the most probable time, representing the relevant time scale of the problem. In the opposite limit $\kappa \rightarrow 0$, β approaches a constant, and the harmonic mean reaction time also reaches a constant. One can check that t_{harm} monotonously decreases as β (or κ) grows.

Figure 6 illustrates by dashed lines the behaviour of the function in (45), in particular, its approach to the limiting expression (46) as κ increases. One can appreciate a very weak dependence of the harmonic mean reaction time for the exterior problem on the reactivity κ . We also show the harmonic mean reaction time in the concentric domain, obtained by a numerical integration in Eq. (40) with $\nu = 1$. This mean significantly depends on κ and behaves as $1/\kappa$ for small κ . Given that the probability density $H(r, t)$ for the concentric domain can be accurately approximated by $H_\infty(r, t)$ at small times (see Eq. (8)), the harmonic mean reaction time for the concentric domain can be approximated by the expression in (40), multiplied by the reaction probability q . This approximation, shown by solid lines, turns out to be remarkably accurate when the target radius ρ is small as compared to the radius R of the confining domain. We can also conclude that the significant variations of t_{harm} with κ for the concentric domain come from those of q with κ .

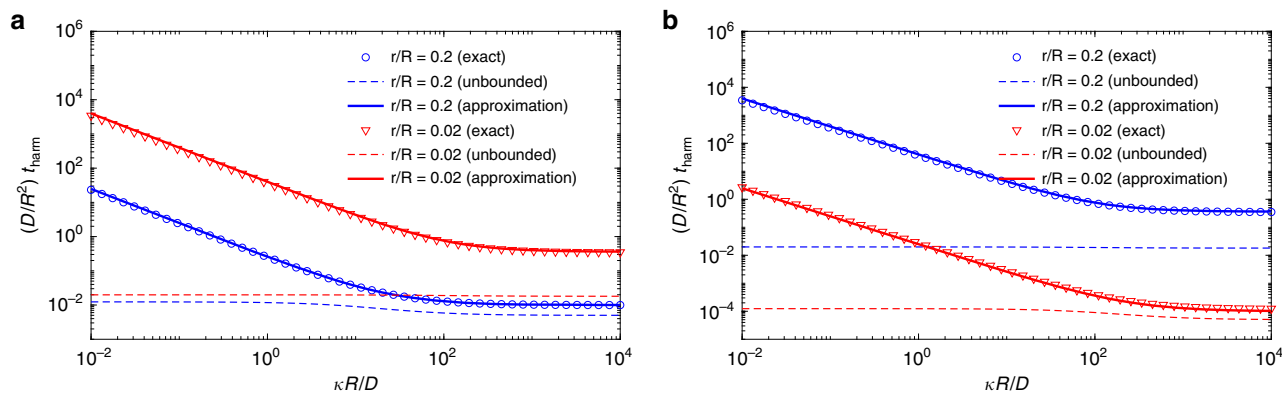


Fig. 6 Harmonic mean reaction time, t_{harm} , as a function of the dimensionless reactivity, $\kappa' = \kappa R/D$. **a** The inner target has a radius $\rho/R = 0.1$ (blue curves) or $\rho/R = 0.01$ (red curves), and the release radius $r/R = 0.2$. Symbols show the results for the concentric domain, obtained by a numerical evaluation of the integral in Eq. (40) with $\nu = 1$; dashed lines present the relation (45) for the exterior problem; solid lines indicate the relation (45) multiplied by the reacting probability q from (41). The length and time units are fixed by setting $R = 1$ and $R^2/D = 1$. **b** The same but for $\rho/R = 0.01$ and two values of r/R : 0.2 (blue curves) and 0.02 (red curves)

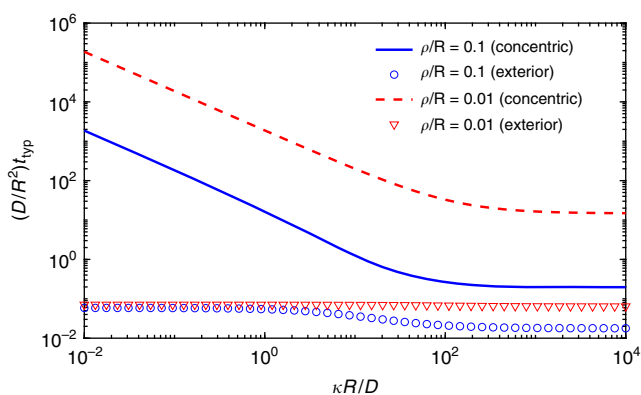


Fig. 7 Logarithmic mean reaction time, t_{typ} , as a function of the dimensionless reactivity, $\kappa R/D$. t_{typ} is evaluated for an inner target of radius $\rho/R = 0.1$ (blue curves) or $\rho/R = 0.01$ (red curves), for the initial radius $r/R = 0.2$. Lines show the results for the concentric domain from Eq. (49), whereas symbols present the relation (52) for the exterior problem. The length and time units are fixed by setting $R = 1$ and $R^2/D = 1$

Finally, we consider the time scale

$$t_{\text{typ}} = t_0 \exp(\langle \ln(t/t_0) \rangle) \quad (47)$$

(where t_0 is an arbitrary time scale), based on the mean logarithm of the reaction time—an important characteristic of the reaction process, which emphasises the typical values of t , i.e., values observed in most of experiments. Indeed, the logarithm is a slowly varying function and its average is supported by the most frequently encountered values of t with the rare anomalously long- or short-reaction times being effectively filtered out. The estimates based on t_{typ} are widely used in the analysis of stochastic reaction-diffusion or transport process in random environments (see, e.g., refs. 40,41 and references therein). Such an averaged value can be formally computed as

$$\begin{aligned} \langle \ln(\tau/t_0) \rangle &= \sum_{n=0}^{\infty} u_n(r) \int_0^{\infty} dt \ln(t/t_0) e^{-Dt \lambda_n} \\ &= - \sum_{n=0}^{\infty} u_n(r) \frac{\gamma + \ln(D t_0 \lambda_n)}{D \lambda_n} \\ &= \left(\ln \frac{(R-\rho)^2}{D t_0} \right) - \gamma - \frac{(R-\rho)^2}{D} \sum_{n=0}^{\infty} u_n(r) \frac{\ln \alpha_n^2}{\alpha_n^2}, \end{aligned} \quad (48)$$

where $\gamma \approx 0.5772\dots$ is the Euler constant, from which

$$t_{\text{typ}} = \frac{(R-\rho)^2}{D} \exp \left(-\gamma - \frac{(R-\rho)^2}{D} \sum_{n=0}^{\infty} u_n(r) \frac{\ln \alpha_n^2}{\alpha_n^2} \right), \quad (49)$$

where $u_n(r)$ are given by (26).

To get a more explicit dependence on the initial radius r , one can again consider the exterior problem ($R = \infty$). Rewriting Eq. (42) as

$$\langle \tau^{-\nu} \rangle_n = \left(\frac{D}{(r-\rho)^2} \right)^{\nu} \frac{2\Gamma(2\nu)}{\Gamma(\nu)} \times \left(1 - \frac{1}{\beta\Gamma(2\nu)} \int_0^{\infty} dz \frac{z^{2\nu} e^{-z}}{1+z/\beta} \right), \quad (50)$$

in order to get a Taylor expansion as $\nu \rightarrow 0$, one finds

$$\langle \ln(\tau/t_0) \rangle_n = \left\{ \ln \left(\frac{(r-\rho)^2}{D t_0} \right) + \gamma + 2e^{\beta} \text{Ei}_1(\beta) \right\}, \quad (51)$$

where the expectation is computed with respect to the renormalised density $H_{\infty}(r, t)/q$. We obtain thus the logarithmic mean time

$$t_{\text{typ}} = \frac{(r-\rho)^2}{D} \exp(\gamma + 2e^{\beta} \text{Ei}_1(\beta)). \quad (52)$$

In the limit $\kappa \rightarrow \infty$, $e^{\beta} \text{Ei}_1(\beta)$ vanishes as $1/\beta$, so that for a perfectly reactive target one gets

$$t_{\text{typ}} = \frac{(r-\rho)^2}{D} e^{\gamma}, \quad (53)$$

which signifies that in the limit $\kappa = \infty$ the logarithmic mean time is comparable to the most probable reaction time t_{mp} .

Figure 7 shows the logarithmic mean reaction time, t_{typ} , as a function of the dimensionless reactivity $\kappa R/D$. As for the harmonic mean in Fig. 6, the results for a bounded concentric domain ($R = 1$) and for the exterior problem ($R = \infty$) differ significantly. The particular definition of the logarithmic time does not allow one to easily renormalise t_{typ} for the exterior domain to get an approximation for the bounded domain.

Finally, Fig. 8 compares several mean reaction times for the concentric domain. One can see that the behaviour of the median, the harmonic and the logarithmic means resembles that of the conventional (arithmetic) mean FPT. In particular, all these means behave as $1/\kappa$ at small κ , indicating that the reaction is limited by the kinetics. Only the most probable FPT exhibits a very different behaviour and shows almost no dependence on the reactivity κ , as discussed above.

Reaction depth. The reaction depth in Eq. (10) is shown in Fig. 9. Note first that the reaction depths corresponding to the shortest characteristic time t_{mp} are evidently the shortest, amounting to only about 4% for perfect reactions and r close to ρ . For finite κ or for starting points further away from the target, the reaction depth $F_r(t_{\text{mp}})$ diminishes. In turn, in all cases the reaction depth connected to the intermediate plateau is dominant, increasingly so due to the reaction-control at lower reactivities.

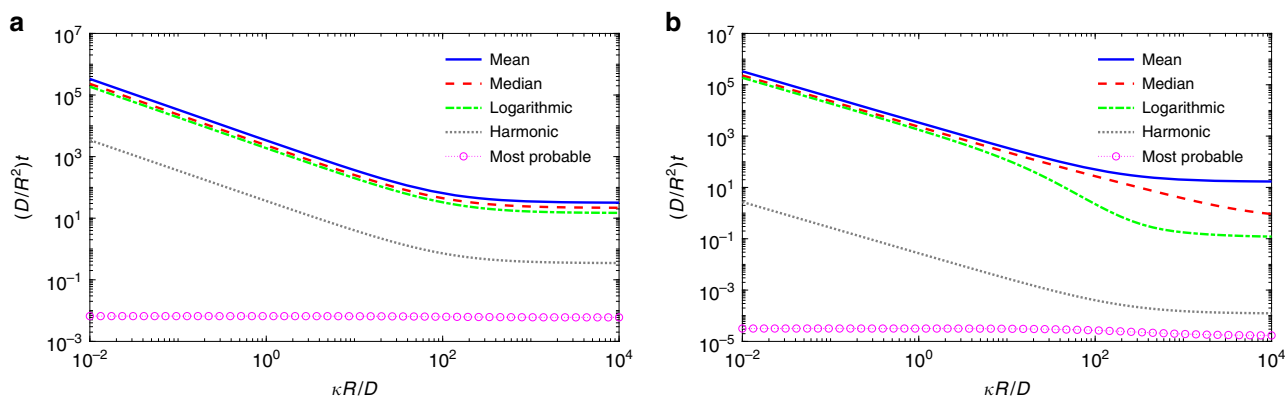


Fig. 8 Comparison of several means of the reaction time. They are evaluated as functions of the normalised reactivity, $\kappa R/D$, for an inner target of radius $\rho/R = 0.01$ and the starting point $r/R = 0.2$ **a** and $r/R = 0.02$ **b**. The length and time units are fixed by setting $R = 1$ and $R^2/D = 1$

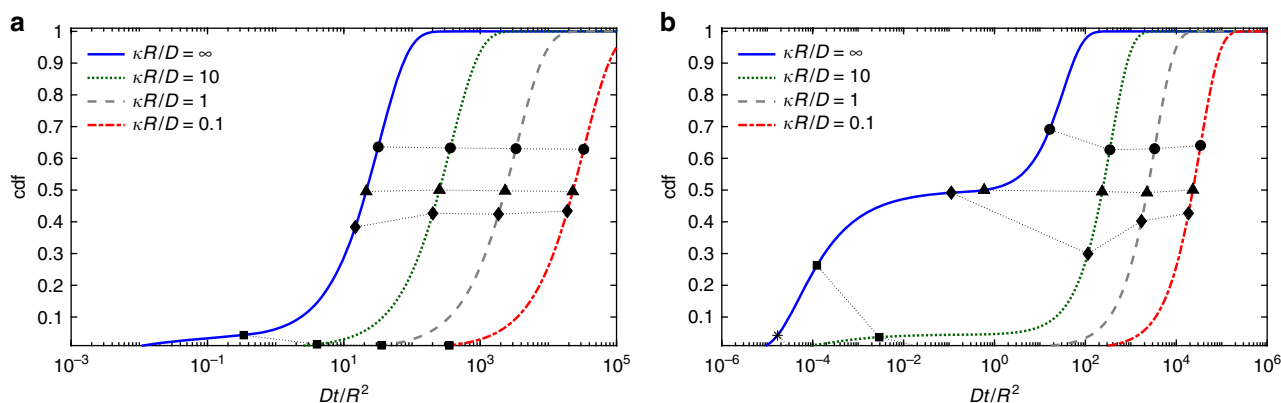


Fig. 9 Cumulative distribution function of reaction times, $F_r(t)$. It is evaluated for the reaction on an inner target of radius $\rho/R = 0.01$, with the starting point **a** $r/R = 0.2$ and **b** $r/R = 0.02$ and varying reactivity κ . Symbols indicate the relevant characteristic times: most probable time t_{mp} (asterisks), harmonic mean t_{harm} (squares), logarithmic mean t_{log} (diamonds), median t_{median} (triangles), and mean time (circles). Note that some most probable times are not seen at this scale

Data and code availability

All figures have been prepared by means of Matlab software. The plotted quantities have been computed by explicit formulas provided in the paper by using custom routines for Matlab software. While the explicit form makes these numerical computations straightforward, custom routines are available from the corresponding author upon request.

Received: 5 September 2018 Accepted: 25 October 2018

Published online: 13 December 2018

References

- Calef, D. F. & Deutch, J. M. Diffusion-controlled reactions. *Ann. Rev. Phys. Chem.* **34**, 493–524 (1983).
- Weiss, G. H. Overview of theoretical models for reaction rates. *J. Stat. Phys.* **42**, 3–36 (1986).
- Shoup, D. & Szabo, A. Role of diffusion in ligand binding to macromolecules and cell-bound receptors. *Biophys. J.* **40**, 33–39 (1982).
- Lindenberg, K., Oshanin, G. & Tachiya, M. Reaction kinetics beyond the textbook: fluctuations, many particle effects and anomalous dynamics. *J. Phys.: Condens. Matter* **19**, 1 (2007).
- Hänggi, P., Talkner, P. & Borkovec, M. Reaction-rate theory: fifty years after Kramers. *Rev. Mod. Phys.* **62**, 251–341 (1990).
- Krapivsky, P. L., Redner, S., & Ben-Naim, E. *A Kinetic View of Statistical Physics* (Cambridge University Press, Cambridge, 2010).
- Oshanin, G. & Burlatsky, S. F. Fluctuation-induced kinetics of reversible coagulation. *J. Phys. A: Math. Gen.* **22**, L973–L976 (1989).
- Oshanin, G., Ovchinnikov, A. A. & Burlatsky, S. F. Fluctuation-induced kinetics of reversible reactions. *J. Phys. A: Math. Gen.* **22**, L977–L982 (1989).
- Yuste, S. B., Oshanin, G., Lindenberg, K., Bénichou, O. & Klafter, J. Survival probability of a particle in a sea of mobile traps: A tale of tails. *Phys. Rev. E* **78**, 021105 (2008).
- Grebenkov, D. S. Searching for partially reactive sites: analytical results for spherical targets. *J. Chem. Phys.* **132**, 034104 (2010).
- Grebenkov, D. S. Subdiffusion in a bounded domain with a partially absorbing-reflecting boundary. *Phys. Rev. E* **81**, 021128 (2010).
- Smoluchowski, M. Versuch einer mathematischen theorie der koagulationskinetik kolloider lösungen. *Z. Phys. Chem.* **92**, 129–168 (1917).
- Collins, F. C. & Kimball, G. E. Diffusion-controlled reaction rates. *J. Colloid Sci.* **4**, 425–437 (1949).
- Sapoval, B. General formulation of Laplacian transfer across irregular surfaces. *Phys. Rev. Lett.* **73**, 3314–3316 (1994).
- Grebenkov, D. S. *Partially Reflected Brownian Motion: A Stochastic Approach to Transport Phenomena*, in “Focus on Probability Theory” (ed. Velle L. R.) 135–169 (Nova Science Publishers, New York, 2006).
- Holcman, D. & Schuss, Z. Control of flux by narrow passages and hidden targets in cellular biology. *Phys. Progr. Rep.* **76**, 074601 (2013).
- Gudowska-Nowak, E., Lindenberg, K. & Metzler, R. Marian Smoluchowski’s 1916 paper – a century of inspiration. *J. Phys. A: Math. Theor.* **50**, 380301 (2017).
- Kolesov, G., Wunderlich, Z., Laikova, O. N., Gelfand, M. S. & Mirny, L. A. How gene order is influenced by the biophysics of transcription regulation. *Proc. Natl. Acad. Sci. USA* **104**, 13948–13953 (2007).
- Pulkkinen, O. & Metzler, R. Distance matters: the impact of gene proximity in bacterial gene regulation. *Phys. Rev. Lett.* **110**, 198101 (2013).
- Alberts, B. et al. *Molecular Biology of the Cell*. (Garland Science, New York, NY, 2014).
- Snustad, D. P. & Simmons, M. J. *Principles of Genetics*. (Wiley, New York, 2000).
- Godec, A. & Metzler, R. Universal proximity effect in target search kinetics in the few-encounter limit. *Phys. Rev. X* **6**, 041037 (2016).

23. Godec, A. & Metzler, R. First passage time distribution in heterogeneity controlled kinetics: going beyond the mean first passage time. *Sci. Rep.* **6**, 20349 (2016).
24. Mejia-Monasterio, C., Oshanin, G., & Schehr, G. First passages for a search by a swarm of independent random searchers, *J. Stat. Mech.* P06022 (2011). <https://doi.org/10.1088/1742-5468/2011/06/P06022>
25. Mattos, T., Mejia-Monasterio, C., Metzler, R. & Oshanin, G. First passages in bounded domains: When is the mean first passage time meaningful? *Phys. Rev. E* **86**, 031143 (2012).
26. Mattos, T., Mejia-Monasterio, C., Metzler, R., Oshanin, G., & Schehr, G. Trajectory-to-trajectory fluctuations in first-passage phenomena in bounded domains, in "First-Passage Phenomena and Their Applications", (eds. Metzler R., Oshanin G., & Redner S.) 203–225. (World Scientific, Singapore, 2014).
27. Redner, S. *A Guide to First Passage Processes*. (Cambridge University press, Cambridge, 2001).
28. Bénichou, O., Chevalier, C., Klafter, J., Meyer, B. & Voituriez, R. Geometry-controlled kinetics. *Nat. Chem.* **2**, 472–477 (2010).
29. Bénichou, O. & Voituriez, R. From first-passage times of random walks in confinement to geometry-controlled kinetics. *Phys. Rep.* **539**, 225–284 (2014).
30. Moffitt, J. R., Chemla, Y. R. & Bustamante, C. Mechanistic constraints from the substrate concentration dependence of enzymatic fluctuations. *Proc. Natl Acad. Sci. USA* **107**, 15739–15744 (2010).
31. Shoup, D., Lipari, G. & Szabo, A. Diffusion-controlled bimolecular reaction rates. *Biophys. J.* **36**, 697–714 (1981).
32. von Hippel, P. H. & Berg, O. Facilitated target location in biological systems. *J. Biol. Chem.* **264**, 675–678 (1989).
33. van Zon, J. S. & ten Wolde, P. R. Simulating biochemical networks at the particle level and in time and space: green's function reaction dynamics. *Phys. Rev. Lett.* **94**, 128103 (2005).
34. Grebenkov, D. S. & Oshanin, G. Diffusive escape through a narrow opening: new insights into a classic problem. *Phys. Chem. Chem. Phys.* **19**, 2723–2739 (2017).
35. Grebenkov, D. S., Metzler, R. & Oshanin, G. Effects of the target aspect ratio and intrinsic reactivity onto diffusive search in bounded domains. *New J. Phys.* **19**, 103025 (2017).
36. Grebenkov, D. S., Metzler, R. & Oshanin, G. Towards a full quantitative description of single-molecule reaction kinetics in biological cells. *Phys. Chem. Chem. Phys.* **20**, 16393–16401 (2018).
37. Gardiner, C. W. *Handbook of Stochastic Methods for Physics, Chemistry and the Natural Sciences* (Berlin, Springer, 1985).
38. Carslaw, H. S. & Jaeger, J. C. *Conduction of Heat in Solids* (Oxford University Press, Oxford, UK, 1959).
39. Oshanin, G., Popescu, M. & Dietrich, S. Active colloids in the context of chemical kinetics. *J. Phys. A: Math. Theor.* **50**, 134001 (2017).
40. Evans, M. R. & Majumdar, S. N. Diffusion with stochastic resetting. *Phys. Rev. Lett.* **106**, 160601 (2011).
41. Dean, D. S., Gupta, S., Oshanin, G., Schehr, G. & Rosso, A. Diffusion in periodic, correlated random forcing landscapes. *J. Phys. A: Math. Theor.* **47**, 372001 (2014).
42. Meyer, B., Chevalier, C., Voituriez, R. & Bénichou, O. Universality classes of first-passage-time distribution in confined media. *Phys. Rev. E* **83**, 051116 (2011).
43. Isaacson, S. A. & Newby, J. Uniform asymptotic approximation of diffusion to a small target. *Phys. Rev. E* **88**, 012820 (2013).

Acknowledgements

D.S.G. acknowledges the support under Grant No. ANR-13-JSV5-0006-01 of the French National Research Agency. RM acknowledges funding from Deutsche Forschungsgemeinschaft (project ME 1535/6-1) and from the Foundation for Polish Science within a Humboldt Polish Honorary Research Scholarship. The authors acknowledge the support of Deutsche Forschungsgemeinschaft (German Research Foundation) and Open Access Publication Fund of Potsdam University.

Author contributions

D.S.G., R.M. and G.O. formulated the problem. D.S.G. performed the mathematical derivations and prepared the figures. D.S.G., R.M. and G.O. analysed the obtained results and wrote the paper.

Additional information

Competing interests: The authors declare no competing interests.

Reprints and permission information is available online at <http://npg.nature.com/reprintsandpermissions/>

Publisher's note: Springer Nature remains neutral with regard to jurisdictional claims in published maps and institutional affiliations.



Open Access This article is licensed under a Creative Commons Attribution 4.0 International License, which permits use, sharing, adaptation, distribution and reproduction in any medium or format, as long as you give appropriate credit to the original author(s) and the source, provide a link to the Creative Commons license, and indicate if changes were made. The images or other third party material in this article are included in the article's Creative Commons license, unless indicated otherwise in a credit line to the material. If material is not included in the article's Creative Commons license and your intended use is not permitted by statutory regulation or exceeds the permitted use, you will need to obtain permission directly from the copyright holder. To view a copy of this license, visit <http://creativecommons.org/licenses/by/4.0/>.

© The Author(s) 2018